

Multi-Tiered Self-Contrastive Learning for Medical Microwave Radiometry (MWR) Breast Cancer Detection

Christoforos Galazis¹, Huiyi Wu², and Igor Goryanin^{3,4,5,*}

¹Department of Computing, Imperial College London, London, United Kingdom

²National Heart & Lung Institute, Imperial College London, London, United Kingdom

³School of Informatics, University of Edinburgh, Edinburgh, United Kingdom

⁴Okinawa Institute Science and Technology, Okinawa, Japan

⁵MMWR LTD, United Kingdom

*igor.goryanin@ed.ac.uk

Abstract

The pursuit of enhanced breast cancer detection and monitoring techniques is a paramount healthcare objective, driving the need for innovative imaging technologies and diagnostic approaches. This study introduces a novel multi-tiered self-contrastive model tailored for the application of microwave radiometry (MWR) breast cancer detection. Our approach encompasses three distinct models: Local-MWR (L-MWR), Regional-MWR (R-MWR), and Global-MWR (G-MWR), each engineered to analyze varying sub-regional comparisons within the breasts. These models are cohesively integrated through the Joint-MWR (J-MWR) network, which leverages the self-contrastive data generated at each analytical level to enhance detection capabilities. Employing a dataset comprising 4,932 cases of female patients, our research showcases the effectiveness of our proposed models. Notably, the J-MWR model distinguishes itself by achieving a Matthews correlation coefficient of 0.74 ± 0.018 , surpassing existing MWR neural networks and contrastive methods. These results highlight the significant potential of self-contrastive learning techniques in improving both the diagnostic accuracy and generalizability of MWR-based breast cancer detection processes. Such advancements hold considerable promise for further investigative and clinical endeavors. The source code is available at: https://github.com/cgalaz01/self_contrastive_mwr

Keywords Self-contrastive learning; Hierarchical neural networks; Medical microwave radiometry; Point-of-care testing; Breast cancer detection

1 Introduction

Breast cancer, marked by the uncontrolled and rapid growth of cells due to genetic mutations, significantly impacts global health, as it records one of the highest incidence rates of cancer. In 2020 alone, it was estimated to account for 2.3 million new cases, becoming the primary cause of death among women with nearly 700,000 deaths [1]. Disturbingly, future forecasts suggest a continued rise in both the occurrence and death rates associated with breast cancer [2].

The pivotal role of early detection in reducing mortality rates and reducing the healthcare load cannot be overstated. In this context, Microwave Radiometry (MWR) emerges as a promising imaging modality that passively captures the natural microwave emissions of human tissues [3]. Its utility spans a broad spectrum of clinical areas, including but not limited to, the breasts [3, 4, 5, 6], brain [7, 8], lungs [9], veins [10], and musculoskeletal structures [11]. Within the domain of breast cancer screening, MWR leverages the fact that cancerous tissues, due to their increased metabolic rate, emit more heat than normal tissue [4]. Its advantages are manifold, offering non-invasive, safe, mobile, and economical options for diagnosis. However, the relatively novel integration of MWR into breast cancer diagnostics introduces challenges, particularly in data interpretation and the integration of this technology into existing medical workflows. Overcoming these hurdles necessitates the deployment of artificial intelligence (AI) models to refine and streamline the application of MWR in a clinical setting.

In the landscape of algorithmic advancements, the last few years have witnessed a surge in efforts to refine MWR breast cancer diagnostic accuracy through various machine-learning models and neural networks. Studies from [12, 13, 14] have shed light on the potency of conventional machine learning strategies, including support vector machines (SVM), random forest algorithms, and Bayesian classifiers, in enhancing diagnostic precision. Parallel to these conventional methods, a range of neural networks have been evaluated and found to deliver promising outcomes, as documented in [12, 13, 15, 16].

Taking a step further, research from [17] proposed a learnable architecture designed not only to bolster diagnostic accuracy but also to pave the way for more efficient, lightweight neural network structures for MWR. This approach underscores a pivotal shift towards creating more resource-efficient models without compromising performance. Furthermore, [6] combined Kohonen’s self-organizing maps with machine learning algorithms, marking a noteworthy stride towards improving the efficacy of these systems. Additionally, the domain of fuzzy analysis has not been left untapped, with studies [18, 19] delving into its applicability and effectiveness.

Before data-driven methods were utilized, a set of hand-engineered features had been proposed [20, 21, 5] based on prior knowledge to identify temperature disparities within the breast. These features, aimed at mammary gland analysis, can be categorized into five groups: 1) temperature asymmetry between the two glands; 2) increased temperature dispersion within a single gland; 3) detection of abnormally high temperatures in the nipple compared to other gland areas; 4) relationship between surface and depth temperature measurements; and 5) features derived from comparing the two glands.

On the other hand, in supervised learning the emphasis lies in comparing across samples of the dataset [22] rather than within the sample itself. This approach is termed supervised contrastive learning, where the learned embedding representation of the data ensures that instances with the same label are brought closer together, while those with different labels are pushed further apart. Research in this domain has predominately focused on how to sample the pair to compare against within the batch. The simplest form is the contrastive loss [23], in which a random negative sample is taken. This has been extended to a triplet loss [24, 25], in which a positive and negative is sampled. A further extension is an N-pair loss [26] where one positive is taken and $N - 1$ negative samples. One of the advantages of employing this learning strategy is the enhanced performance and generalizability of the resulting models [22].

However, despite notable advancements in developing models for MWR breast cancer detection, a critical challenge persists in the seamless integration of data-driven methodologies with existing knowledge, including hand-engineered features [20, 21]. The incorporation of such prior knowledge into the models is pivotal to improving the performance and generalizability. Such advancements are paramount for MWR’s application in the clinical setting amidst varying and evolving conditions.

In this paper, we introduce a novel supervised neural network known as the Joint-MWR (J-MWR), which embodies hierarchical self-contrastive models. Unlike traditional approaches, it learns by comparing different regions within itself rather than across different cases. This innovative model aims to enhance the analysis of sub-regions across both breasts through a unified structure. Our methodology employs a tri-tiered comparative analysis strategy to enhance the detection capabilities of the MWR breast cancer detection system. We demonstrate that the J-MWR surpasses both the state-of-the-art MWR model and widely used batch-wise contrastive learning methods, highlighting its superior performance.

At the initial stage, the Local-MWR (L-MWR) comparison occurs, where each point within the breast undergoes comparison against every other point, enabling a detailed analysis. The next tier, Regional-MWR (R-MWR), focuses on comparing corresponding points between the two breasts, aiming to identify symmetry or anomalies between them. Finally, at the Global-MWR (G-MWR) tier, each breast undergoes mirroring, swapping roles to contrast and compare, thereby revealing subtle variations and collective patterns.

This layered approach replicates traditional comparison techniques utilized in hand-engineered feature extraction within a data-centric framework. Consequently, it enriches the MWR breast cancer detection system with enhanced robustness and adaptability, rendering it a more versatile tool in combating breast cancer.

In summary, our contributions are twofold: 1) We introduce a novel supervised multi-tiered self-contrastive framework, enabling comparison of regions within itself, and 2) We evaluate, for the first time, the performance of batch-wise contrastive learning on a large MWR dataset.

2 Materials and Methods

2.1 Data

The data for this study was gathered using the point-of-care MWR-2020 dual-band device manufactured by MMWR Ltd¹. This device monitors both infrared (skin temperature) and microwave (internal tissue temperature) emissions. Operating within a microwave frequency range of 3.5 to 4.2 GHz, it can penetrate tissues to depths ranging from 3 to 7 cm. The acquisition accuracy for temperature measurements obtained from the infrared and microwave antennas is within $\pm 0.2^{\circ}\text{C}$.

Each case in the study involved the measurement of 22 locations, which can be seen in Figure 1. Specifically, for each breast, eight points were measured equidistantly around the nipple, including the nipple itself. Additionally, a single point was measured in the left and right axillary reference regions. Two additional points were recorded under the chest to serve as reference points. At each of these 22 locations, both skin and internal temperatures were recorded, resulting in a total of 44 temperature readings per case, which serve as the models' input.

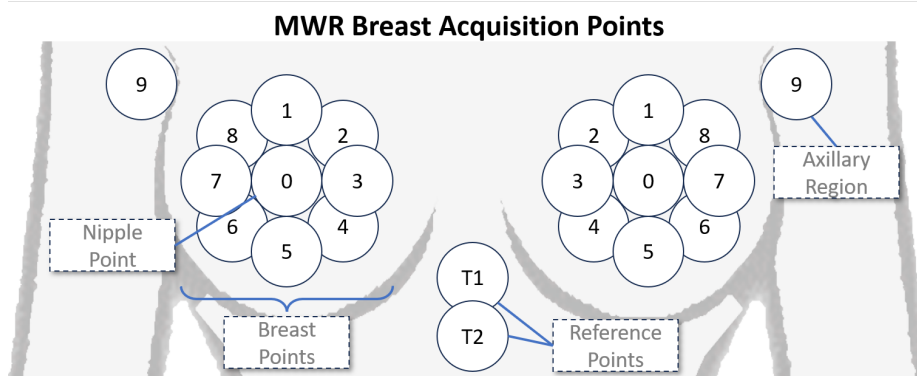


Figure 1: An illustration of the skin and internal acquisition points on the breasts. Point 0 is on the nipple, points 1-8 are equidistantly around the nipple, point 9 is on the axillary region, and points T1 and T2 are under the chest.

The data was collected with ethical approval, and consent from participants and fully anonymized. In total, the dataset comprises measurements from 4,932 female cases across multiple clinical centers. Among these cases, 4,384 were deemed healthy by clinical experts, while the remaining 548 were classified as cancerous, with an example of each can be seen in Figure 2. The data was randomly class-balanced split into training, validation, and testing sets, constituting 60%, 20%, and 20% of the entire dataset, respectively. Model evaluation was conducted on the test set, with test results generated upon completion of the development and experimentation phases.

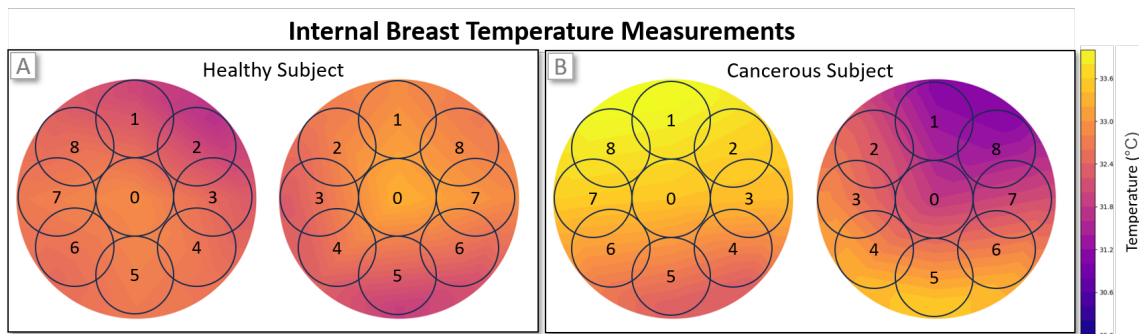


Figure 2: Comparison of internal breast temperature profiles between a healthy (Panel A) and high growth rate cancerous (Panel B) case. In the healthy instance, no significant temperature asymmetries are evident. However, in the cancerous case, notably elevated temperatures are observed in regions 1 and 8 of the left-hand side gland.

¹<https://www.mmwr.co.uk/>

2.2 Models

We standardized the model settings utilized across all presented models. Initialization of model weights employed Glorot uniform initialization [27], with initial biases set to 0. Weight optimization utilized the Adam optimizer [28] with an initial learning rate of 0.0001, and the remaining parameters, β_1 , and β_2 set to 0.9 and 0.999, respectively. The learning rate was reduced by a factor of 0.1 if the validation loss did not decrease after 5 epochs. A batch size of 4 was determined to be suitable for all evaluated models. The weights were updated based on the class-balanced binary cross-entropy loss.

2.3 Base Model

To streamline our approach, we introduce a fundamental building block called the MWR-Block, which is a residual fully connected (FC) component outlined in Figure 3A. Each MWR-Block consists of an FC layer, layer normalization, a Rectified Linear Unit (ReLU) activation function [29], another FC layer, layer normalization, ReLU, and addition with the block’s input.

Our baseline model, hereafter defined as the "base model", is the neural network proposed in [12]. However, to accommodate the larger dataset under evaluation, we made adjustments to the base model’s parameters. Specifically, it now comprises 4 MWR-Blocks, each FC layer containing 256 units. The output FC layer of unit size 1 uses a sigmoid activation function.

2.4 Self-Contrastive MWR Neural Networks

Inward learning, not outward wandering Our proposed models utilize self-contrastive learning to optimize the embedding space for distinguishing between healthy and cancerous samples. The embedding space of healthy and cancerous cases is pushed to distinct clusters. Unlike traditional contrastive learning methods, our approach focuses on features within individual cases rather than across samples.

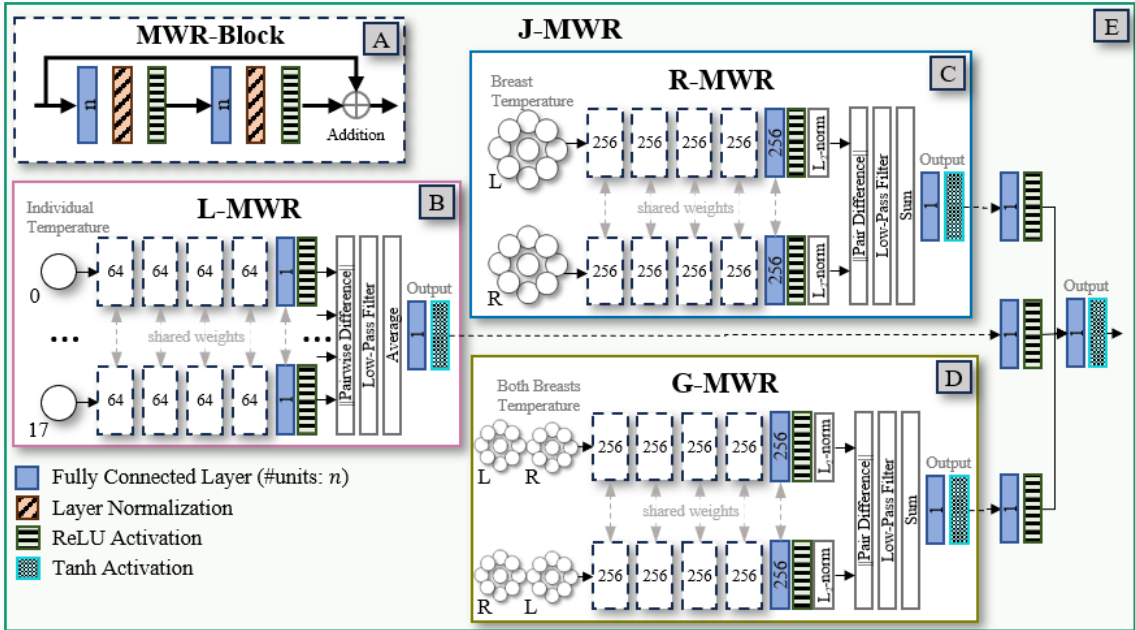


Figure 3: Overview of the proposed multi-tiered self-contrastive MWR models for breast cancer detection. **A)** The common residual block used in all networks, MWR-Block. **B)** L-MWR network that compares all individual points between them. **C)** R-MWR network that compares between the left and right breasts. **D)** G-MWR network that compares both breasts with their positional inverse self. **E)** J-MWR network that combines all previous models to obtain a new prediction.

2.4.1 L-MWR Neural Network

The Local-MWR (L-MWR) network processes each temperature point individually, excluding reference measurements, resulting in 18 inputs, each consisting of skin and internal values (see Figure

3B). The network is structured into feature extraction and feature comparison. Feature extraction involves 4 MWR-Blocks, followed by a single unit FC layer with ReLU activation, in which the weights are shared. Small activations below a learnable threshold are filtered to 0. Feature comparison computes the mean absolute feature differences between pairwise inputs. The prediction is obtained through a single unit FC layer with the tanh activation function, as the activations are already bound below to 0.

2.4.2 R-MWR Neural Network

The Regional-MWR (R-MWR) network compares left and right breasts as self-contrastive regions (see Figure 3C), with 2 inputs of vector size 24 each, including respective breast and reference points. Shared feature extraction includes 4 MWR-Blocks with 256 units, followed by an FC layer with ReLU activation, and l_2 normalization. Element-wise absolute differences are computed, filtered, and summed for comparison. Prediction is generated via a single unit FC layer with tanh activation.

2.4.3 G-MWR Neural Network

The Global-MWR (G-MWR) network utilizes features from both breasts (see Figure 3D). However, to perform self-contrastive learning, we use as the second input the inverse positions, in which the values of the left breast are used as the right and vice versa. Thus, G-MWR takes two pairs of input, each of size 44, and uses the same architecture as R-MWR, described in section 2.4.2.

2.4.4 J-MWR Neural Network

The Joint-MWR (J-MWR) network combines the L-MWR (section 2.4.1), R-MWR (section 2.4.2), and G-MWR (section 2.4.3) pre-trained models to leverage their complementary features (see Figure 3E). Weighted outputs from each sub-network, using individual FC layers, are concatenated and passed through a final single unit FC layer with tanh activation. As we are only fine-tuning the weights of the sub-networks, the learning rate was reduced to $1e-7$.

2.5 Experiments

In our experiments, we conducted three model executions with different initialization seeds, and the reported results represent the average across these three seeds on the test set. The model evaluation is based on the Matthews correlation coefficient (MCC) to assess the performance of imbalanced data when we consider both positive and negative cases equally important [30]. We also assessed the accuracy and receiver operating characteristic (ROC) area under the curve (AUC) for the main results as a reference. Our analysis involved comparing our proposed self-contrastive models with commonly used batch-wise contrastive losses, both individually and in combination.

Specifically, we utilized contrastive loss [23], triplet hard loss [24], triplet semi-hard loss [25], and N-pairs loss [26], where N is the number of negatives in the batch. The weight assigned to the batch-wise contrastive losses was experimentally determined to be 0.1, while the weight for cross-entropy classification remained at 1.0.

3 Results

3.1 Model Evaluation

Our proposed J-MWR model has the highest predictive capabilities in correctly identifying breast cancer from MWR data. It obtains an MCC score of 0.74 ± 0.018 , a 0.08 margin from the second-best performing model, R-MWR. This translates to an accuracy of 0.95 ± 0.003 and an ROC AUC of 0.96 ± 0.001 . In comparison, the base model obtains an MCC score of 0.58 ± 0.004 , an accuracy of 0.88 ± 0.003 , and an ROC AUC of 0.93 ± 0.006 . The results for all models can be seen in Table 1.

We can consider J-MWR as a meta-classifier of the sub-networks. In this case, when we compare individual models, we can observe that both R-MWR and G-MWR outperform the base model with an MCC of 0.66 ± 0.012 and 0.61 ± 0.045 , respectively. L-MWR is the only model that performs substantially worse than the base model, with an MCC score of 0.43 ± 0.002 . This is expected as the model only learns features from a single point.

Table 1: The mean and standard deviation of accuracy, MCC, and ROC AUC for the base model, and the proposed models L-MWR, R-MWR, G-MWR, and J-MWR.

Model	Accuracy	MCC	ROC AUC
Base	0.88 ± 0.003	0.58 ± 0.004	0.93 ± 0.006
L-MWR	0.82 ± 0.002	0.43 ± 0.002	0.89 ± 0.001
R-MWR	0.92 ± 0.003	0.66 ± 0.012	0.95 ± 0.006
G-MWR	0.90 ± 0.021	0.61 ± 0.045	0.94 ± 0.016
J-MWR	0.95 ± 0.003	0.74 ± 0.018	0.96 ± 0.001

3.2 Batch-wise Contrastive Loss Evaluation

When employing batch-wise contrastive loss, J-MWR with triplet hard loss achieves the highest performance, as illustrated in Table 2, with an MCC score of 0.74 ± 0.03 . Overall, J-MWR consistently achieves the highest MCC score compared to other models, regardless of the batch-wise contrastive loss used. However, none of the configurations surpass J-MWR without batch-wise contrastive learning.

Interestingly, both R-MWR and J-MWR experience a reduction in MCC score when utilizing batch-wise contrastive learning. On the other hand, L-MWR shows a slight improvement of 0.01, while G-MWR demonstrates an improvement ranging from 0.03 to 0.06. The base model also benefits from contrastive and N-pairs losses, with an MCC score increase of 0.02 for both configurations.

Table 2: The mean and standard deviation MCC results of each model when trained using a batch-wise contrastive loss (contrastive, N-pairs, triplet hard, and triplet semi-hard). MCC values in **bold** indicate an improvement over their non-batch-wise loss counterparts.

Model	MCC			
	Contrastive	N-pairs	Triplet hard	Triplet semi-hard
Base	0.60 ± 0.024	0.60 ± 0.035	0.57 ± 0.016	0.51 ± 0.149
L-MWR	0.44 ± 0.003	0.44 ± 0.001	0.44 ± 0.004	0.44 ± 0.008
R-MWR	0.63 ± 0.060	0.59 ± 0.019	0.60 ± 0.026	0.64 ± 0.025
G-MWR	0.65 ± 0.005	0.64 ± 0.012	0.64 ± 0.022	0.67 ± 0.017
J-MWR	0.71 ± 0.000	0.71 ± 0.029	0.74 ± 0.030	0.70 ± 0.081

3.3 Embedding Space

In this analysis, we explore the properties and characteristics of the embedding space generated by the L-MWR, R-MWR, G-MWR, and base contrastive models. The 2D projections of the embedding spaces can be observed in Figure 4. Our findings reveal that the base contrastive model, in comparison to our proposed models, excels at delineating a clearer boundary between the healthy and cancerous groups, with a mean between-class distance of 6.57 ± 3.71 . This result is expected, given its explicit training for this task. However, notable disparities within the groups emerge, as reflected by a mean within-class distance of 4.53 ± 2.85 , contributing to its relatively lower performance.

Our proposed models, despite being trained on comparing features within themselves, we observe that cancerous cases tend to have similar embedding properties across cases. However, these cases are more intertwined with the healthy cases, making it challenging to discern a clear boundary between them. For instance, R-MWR demonstrates a mean within-class distance of 2.93 ± 1.46 and a mean between-class distance of 3.94 ± 1.17 . This close proximity of each group sufficiently mitigates the lack of a clear boundary, thereby improving performance.

These findings suggest the potential for the two methods, self-contrastive and batch-wise contrastive, to complement each other and further enhance performance.

3.4 Data Constraint Training

We retrained the models using randomly selected subsets of the training set at 75%, 50%, and 25%. This approach allows us to gauge how the models perform when trained with limited data, offering insights into their scalability as more data becomes available. The performance of the models is summarized in Figure 5a. J-MWR consistently demonstrates the highest MCC across all subsets,

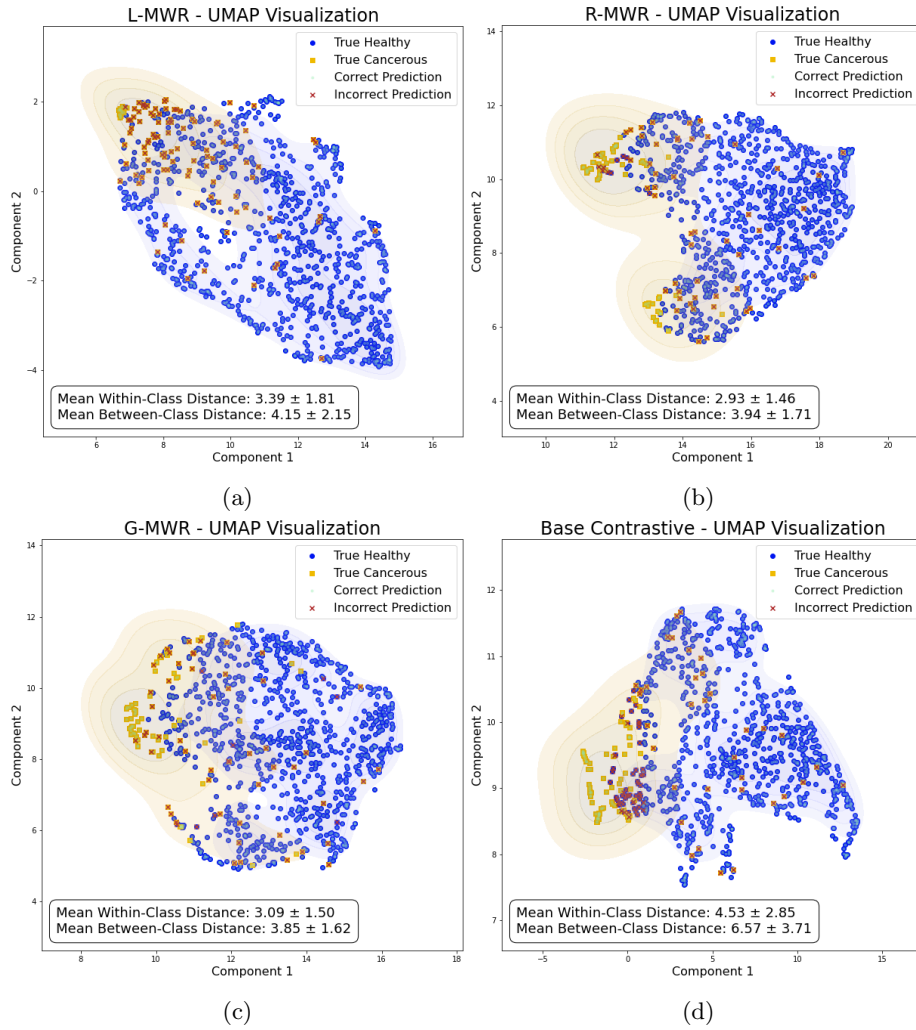


Figure 4: Uniform Manifold Approximation and Projection (UMAP) [31] embedding visualizations of (a) L-MWR, (b) R-MWR, (c) G-MWR, and (d) base contrastive are presented. In each figure, a blue circle indicates a correct healthy prediction, a yellow square signifies a correct cancerous prediction and a red cross overlaid on the previous cases indicates a respective incorrect prediction.

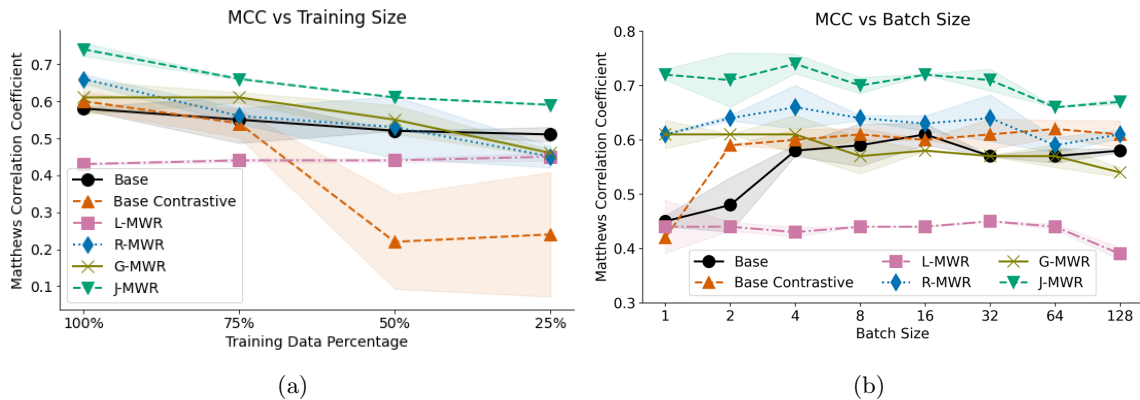


Figure 5: (a) MCC scores of each of the models as the training size is reduced to 75%, 50%, and 25% of the original size. (b) MCC scores of the models as the batch size changes from 1 to 128.

obtaining its lowest value of 0.59 ± 0.001 at 25%. In contrast, the base contrastive model exhibits its lowest performance at 50% and 25% training percentages but notably improves at 75%. Remarkably, L-MWR maintains a consistent level of performance regardless of the reduction in training data size. Between 75% to 100% of the training data, R-MWR shows the highest performance gain of 0.1 MCC, highlighting its effective utilization of additional data, which also reflects upon J-MWR. The

performance of the remaining models appears to plateau as more training data is added.

3.5 Batch Size Dependency

In our investigation into the impact of batch size on performance, we analyzed values ranging from 1 to 128. J-MWR consistently outperforms other models, achieving its peak MCC at a batch size of 4 with a value of 0.74 ± 0.018 , followed by a gradual decline, as shown in Figure 5b. Notably, while most models experienced a decline in performance with increasing batch size, the base contrastive model maintained near-consistent performance levels, a trend we anticipate extending to larger batch sizes.

This suggests that, for self-contrastive models, smaller batch sizes are preferable, although this comes with a trade-off between training speed and accuracy. Smaller batches may yield higher accuracy but result in longer training times. In contrast, batch-wise contrastive losses for MWR are less influenced by batch size.

3.6 Generalizability

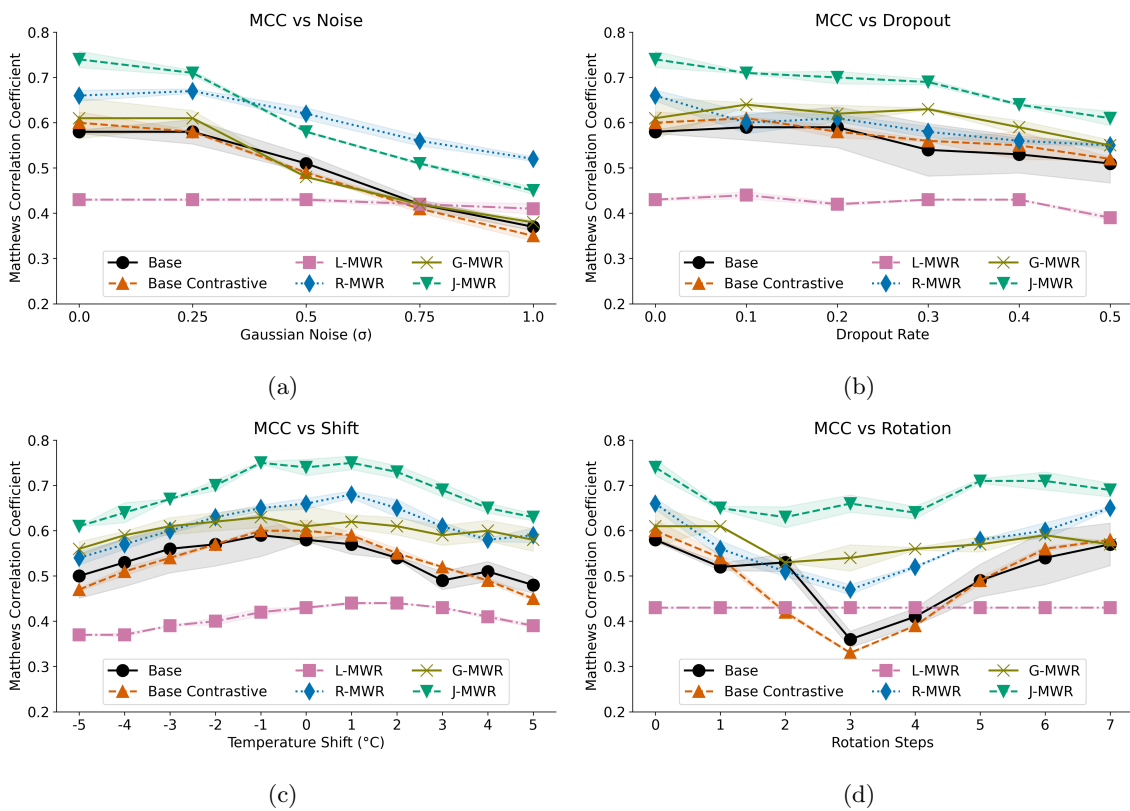


Figure 6: MCC scores of the models as we add increasing amounts of Gaussian noise (a), randomly set points to the mean of the remaining (b), shift all the temperatures by a given amount (c) and rotate the points around the nipple of each breast (d).

To assess the generalizability of our trained models, we subjected them to an augmented test set comprising various out-of-distribution transformations. These transformations included adding Gaussian noise (Figure 6a), applying dropout to the temperature points and setting their value to the mean of the remaining points (Figure 6b), adjusting the temperature of all values (Figure 6c), and rotating the breast points around the nipple (Figure 6d).

As depicted in Figure 6, J-MWR consistently demonstrated better generalization performance, evidenced by its higher MCC score compared to other models, both in the presence of data corruptions (Figures 6a and 6b) and data drifts (Figures 6c and 6d). However, when subjected to large Gaussian noise ($\sigma > 0.25$), R-MWR showed greater resilience. This decline in J-MWR’s performance can be attributed to the poorer performance of G-MWR under noisy conditions. We note that while L-MWR shows the smallest changes across the different transformations its performance

remains low at around 0.43 MCC. However, under some conditions (see Figure 6) it can outperform the base, base contrastive, and/or G-MWR models.

Overall, these findings underscore the robustness of J-MWR in handling various forms of data perturbations, albeit with some sensitivity to specific types of noise. Comparing regions within the individual case rather than across samples allows it to better generalize to unknown distributions.

3.7 Ensemble Methods

In the J-MWR network, each sub-network contributes almost equally to the final prediction. Specifically, the L-MWR, with a weight of 0.998, holds comparable significance to both the R-MWR and G-MWR networks, each possessing weights close to 1.0. Moreover, their biases are all approximately 0. From Figure 7, it is apparent that J-MWR surpasses other ensemble techniques, including averaging and majority voting, as well as meta-classifiers such as logistic regression, SVM, and decision tree. While J-MWR bears a resemblance to averaging voting, the fine-tuning step applied to the sub-networks enables substantial enhancement in MCC performance.

When averaging the predictions of L-MWR, R-MWR, and G-MWR, the second-best MCC value of 0.66 ± 0.02 is achieved, which is comparable to that obtained from R-MWR alone. Following closely is the majority voting approach. Notably, despite best efforts, the remaining meta-classifiers exhibited overfitting to the training data, leading to a large decline in MCC performance on the test set.

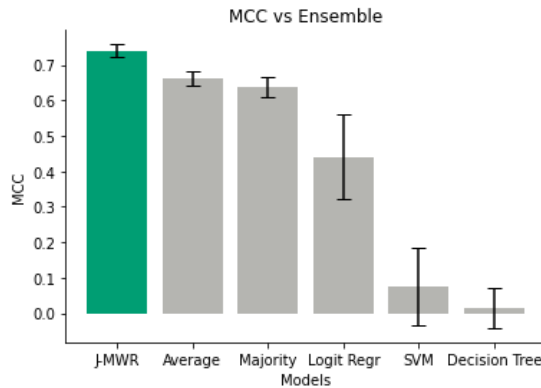


Figure 7: MCC scores on different ensemble methods using the pre-trained L-MWR, R-MWR, and G-MWR models.

4 Discussion

In this study, we have demonstrated the successful adaptation of self-contrastive learning to tackle MWR breast cancer detection. Our proposed architectures, namely L-MWR, R-MWR, and G-MWR, offer a novel approach to integrating hand-engineered features capturing thermal asymmetries alongside data-driven methods. Our combined model, J-MWR, achieves an MCC score of 0.74 ± 0.018 surpassing all existing models, showcasing its efficacy in detecting breast cancer with high accuracy and generalizability. This underscores the potential of self-contrastive learning in enhancing the performance of breast cancer detection systems.

The final layer of J-MWR acts as an ensemble averaging due to the weights of each sub-network being near 1. However, J-MWR gains an improvement of 0.08 MCC compared to the traditional ensemble averaging. This improvement is attributed to the fact that J-MWR serves as a fine-tuning meta-classifier. Specifically, it enables the indirect sharing of information between each self-contrastive tier, thereby enhancing performance. However, it's important to note that this benefit comes at the cost of increased model complexity.

Furthermore, batch-wise contrastive learning, while it only contributed to minor improvements, we see potential in its use. It presents a minimally disruptive enhancement to existing MWR models. Our future efforts will focus on refining positive and negative sampling strategies tailored to physiological characteristics, thus advancing beyond mere classification considerations. Its current subpar performance can be attributed to the inherent variability in breast temperature readings, influenced by factors such as age and menstrual cycle phase [3].

Furthermore, while batch-wise contrastive learning only resulted in minor improvements, we recognize its potential value. It offers a minimally disruptive enhancement to existing MWR models. Our future efforts will concentrate on refining positive and negative sampling strategies tailored to the physiological characteristics of the breasts, thus advancing beyond mere classification considerations. The current subpar performance of batch-wise contrastive learning can be attributed to the inherent variability in breast temperature readings, influenced by factors such as age and menstrual cycle phase [3].

5 Conclusion

Our research presents promising advancements in MWR breast cancer detection, offering potential clinical benefits and avenues for future exploration. Moving forward, further refinement through NAS and tailored sampling strategies holds promise for further enhancing diagnostic accuracy. Additionally, evaluating our proposed model across various anatomical locations and under different physiological conditions will be crucial for expanding its applicability and effectiveness in diverse clinical settings. To further improve breast cancer predictions, we aim to adapt our proposed self-contrastive learning approach by including mammogram, gene expression, miRNA and other multi-omics data.

References

- [1] H. Sung, J. Ferlay, R. L. Siegel, M. Laversanne, I. Soerjomataram, A. Jemal, and F. Bray, “Global cancer statistics 2020: Globocan estimates of incidence and mortality worldwide for 36 cancers in 185 countries,” *CA: a cancer journal for clinicians*, vol. 71, no. 3, pp. 209–249, 2021.
- [2] M. Arnold, E. Morgan, H. Rungay, A. Mafra, D. Singh, M. Laversanne, J. Vignat, J. R. Gralow, F. Cardoso, S. Siesling, and I. Soerjomataram, “Current and future burden of breast cancer: Global statistics for 2020 and 2040,” *The Breast*, vol. 66, pp. 15–23, 2022.
- [3] I. Goryanin, S. Karbainov, O. Shevelev, A. Tarakanov, K. Redpath, S. Vesnin, and Y. Ivanov, “Passive microwave radiometry in biomedical studies,” *Drug Discovery Today*, vol. 25, no. 4, pp. 757–763, 2020.
- [4] S. Vesnin, A. K. Turnbull, J. M. Dixon, and I. Goryanin, “Modern microwave thermometry for breast cancer,” *J. Mol. Imaging Dyn*, vol. 7, no. 2, p. 1000136, 2017.
- [5] L. Fisher, O. Fisher, D. Chebanov, S. Vesnin, A. Goltsov, A. Turnbull, M. Dixon, I. Kudaibergenova, B. Osmonov, S. Karbainov, L. Popov, A. Losev, and I. Goryanin, “Passive microwave radiometry and microrna detection for breast cancer diagnostics,” *Diagnostics*, vol. 13, no. 1, p. 118, 2022.
- [6] A. V. Khoperskov and M. V. Polyakov, “Improving the efficiency of oncological diagnosis of the breast based on the combined use of simulation modeling and artificial intelligence algorithms,” *Algorithms*, vol. 15, no. 8, p. 292, 2022.
- [7] O. Shevelev, M. Petrova, A. Smolensky, B. Osmonov, S. Toimatov, T. Kharybina, S. Karbainov, L. Ovchinnikov, S. Vesnin, A. Tarakanov, and I. Goryanin, “Using medical microwave radiometry for brain temperature measurements,” *Drug discovery today*, vol. 27, no. 3, pp. 881–889, 2022.
- [8] O. A. Shevelev, M. V. Petrova, E. M. Mengistu, M. Y. Yuriev, I. Z. Kostenkova, S. G. Vesnin, M. M. Kanarskii, M. A. Zhdanova, and I. Goryanin, “Correction of local brain temperature after severe brain injury using hypothermia and medical microwave radiometry (mwr) as companion diagnostics,” *Diagnostics*, vol. 13, no. 6, p. 1159, 2023.
- [9] B. Osmonov, L. Ovchinnikov, C. Galazis, B. Emilov, M. Karaibragimov, M. Seitov, S. Vesnin, A. Losev, V. Levshinskii, I. Popov, C. Mustafin, T. Kasymbekov, and I. Goryanin, “Passive microwave radiometry for the diagnosis of coronavirus disease 2019 lung complications in kyrgyzstan,” *Diagnostics*, vol. 11, no. 2, p. 259, 2021.
- [10] V. Levshinskii, C. Galazis, A. Losev, T. Zamechnik, T. Kharybina, S. Vesnin, and I. Goryanin, “Using ai and passive medical radiometry for diagnostics (mwr) of venous diseases,” *Computer Methods and Programs in Biomedicine*, vol. 215, p. 106611, 2022.

- [11] A. V. Tarakanov, E. S. Ladanova, A. A. Lebedenko, T. D. Tarakanova, S. G. Vesnin, T. Kharybina, and I. I. Goryanin, “Passive microwave radiometry as a component of imaging diagnostics in juvenile idiopathic arthritis,” *Rheumato*, vol. 2, no. 3, pp. 55–68, 2022.
- [12] V. Levshinskii, C. Galazis, L. Ovchinnikov, S. Vesnin, A. Losev, and I. Goryanin, “Application of data mining and machine learning in microwave radiometry (mwr),” in *Biomedical Engineering Systems and Technologies: 12th International Joint Conference, BIOSTEC 2019, Prague, Czech Republic, February 22–24, 2019, Revised Selected Papers 12*. Springer, 2020, pp. 265–288.
- [13] C. Galazis, S. Vesnin, and I. Goryanin, “Application of artificial intelligence in microwave radiometry (mwr).” in *Bioinformatics*, 2019, pp. 112–122.
- [14] A. Losev, I. Popov, A. Y. Petrenko, A. Gudkov, S. Vesnin, and S. Chizhikov, “Some methods for substantiating diagnostic decisions made using machine learning algorithms,” *Biomedical Engineering*, vol. 55, no. 6, p. 442, 2022.
- [15] A. G. Losev, D. A. Medvedev, and A. V. Svetlov, “Neural networks in diagnosis of breast cancer,” in *Smart Technologies for Society, State and Economy 13*. Springer, 2021, pp. 220–227.
- [16] A. G. Losev and A. V. Svetlov, “Artificial intelligence algorithms in diagnosis of breast cancer,” in *New Technology for Inclusive and Sustainable Growth: Perception, Challenges and Opportunities*. Springer, 2022, pp. 175–182.
- [17] J. Li, C. Galazis, L. Popov, L. Ovchinnikov, T. Kharybina, S. Vesnin, A. Losev, and I. Goryanin, “Dynamic weight agnostic neural networks and medical microwave radiometry (mwr) for breast cancer diagnostics,” *Diagnostics*, vol. 12, no. 9, p. 2037, 2022.
- [18] I. Germashev, V. Dubovskaya, A. Losev, and I. Popov, “Fuzzy inference of the effectiveness factors of the computational model for the diagnosis of breast cancer,” in *2021 3rd International Conference on Control Systems, Mathematical Modeling, Automation and Energy Efficiency (SUMMA)*. IEEE, 2021, pp. 528–533.
- [19] I. Germashev, V. Dubovskaya, and A. Losev, “Hierarchical fuzzy inference of adequacy of highly informative diagnostic signs of breast cancer,” in *Society 5.0: Cyber-Solutions for Human-Centric Technologies*. Springer, 2023, pp. 31–41.
- [20] A. Zenovich, V. Glazunov, A. Oparin, and F. Primachenko, “Algoritmy prinyatiya resheniy v konsultativnoy intellektualnoy sisteme diagnostiki molochnykh zhelez [algorithms of decision-making in intelligent advisory system for diagnostics of the mammary glands],” *Vestnik Volgogradskogo gosudarstvennogo universiteta. Seriya 1, Matematika. Fizika*, pp. 129–142, 2016.
- [21] A. Losev and V. Levshinskiy, “Intellektualnyy analiz termometricheskikh dannykh v diagnostike molochnykh zhelez [the thermometry data mining in the diagnostics of mammary glands],” *Upravlenie bolshimi sistemami*, no. 70, pp. 113–135, 2017.
- [22] P. Khosla, P. Teterwak, C. Wang, A. Sarna, Y. Tian, P. Isola, A. Maschinot, C. Liu, and D. Krishnan, “Supervised contrastive learning,” *Advances in neural information processing systems*, vol. 33, pp. 18 661–18 673, 2020.
- [23] R. Hadsell, S. Chopra, and Y. LeCun, “Dimensionality reduction by learning an invariant mapping,” in *2006 IEEE computer society conference on computer vision and pattern recognition (CVPR’06)*, vol. 2. IEEE, 2006, pp. 1735–1742.
- [24] A. Hermans, L. Beyer, and B. Leibe, “In defense of the triplet loss for person re-identification,” *arXiv preprint arXiv:1703.07737*, 2017.
- [25] F. Schroff, D. Kalenichenko, and J. Philbin, “Facenet: A unified embedding for face recognition and clustering,” in *Proceedings of the IEEE conference on computer vision and pattern recognition*, 2015, pp. 815–823.
- [26] K. Sohn, “Improved deep metric learning with multi-class n-pair loss objective,” *Advances in neural information processing systems*, vol. 29, 2016.
- [27] X. Glorot and Y. Bengio, “Understanding the difficulty of training deep feedforward neural networks,” in *Proceedings of the thirteenth international conference on artificial intelligence and statistics. JMLR Workshop and Conference Proceedings*, 2010, pp. 249–256.

- [28] D. P. Kingma and J. Ba, “Adam: A method for stochastic optimization,” *arXiv preprint arXiv:1412.6980*, 2014.
- [29] V. Nair and G. E. Hinton, “Rectified linear units improve restricted boltzmann machines,” in *Proceedings of the 27th international conference on machine learning (ICML-10)*, 2010, pp. 807–814.
- [30] D. Chicco and G. Jurman, “The advantages of the matthews correlation coefficient (mcc) over f1 score and accuracy in binary classification evaluation,” *BMC genomics*, vol. 21, pp. 1–13, 2020.
- [31] L. McInnes, J. Healy, and J. Melville, “Umap: Uniform manifold approximation and projection for dimension reduction,” *arXiv preprint arXiv:1802.03426*, 2018.